coatings

MDPI

Article

The Combined Influences of Film Cooling and Thermal Barrier Coatings on the Cooling Performances of a Film and Internal Cooled Vane

Li Shi *, Zhiying Sun and Yuanfeng Lu

School of Mechanical Engineering, Xiangtan University, Xiangtan 411105, China; zhiyinsun@sina.com (Z.S.); xtulyf@126.com (Y.L.)

* Correspondence: shili@xtu.edu.cn; Tel.: +86-731-5829-2209

Received: 10 August 2020; Accepted: 3 September 2020; Published: 5 September 2020



Abstract: This paper presents a numerical investigation on the combined influences of film cooling and thermal barrier coatings (TBCs) on the cooling performances of a NASA C3X guide vane. The results show that: (1) film cooling on the pressure side is more effective than suction side, especially on the trailing edge where multiple cooling and thermal protection techniques include internal cooling and TBCs are necessary. (2) TBCs show positive and negative roles in improving cooling performance at the same time for the coated vane with or without film cooling. Without film cooling, TBCs show negative roles on the regions with lower temperature external hot gas, which is caused by flow acceleration from the stagnation line of the suction side. (3) Internal cooling improvement caused by coolant introduction leads to a larger cooling effectiveness inclement due to TBCs near coolant plenums and film cooling holes. However, the influence of TBCs on cooling effectiveness increment goes down and even shows negative roles on the regions away from coolant plenums and under the effective coverage of the film cooling. (4) Improving the convective heat transfer of coolant with the wall of coolant plenums and film cooling holes is the guarantee of improving the cooling performance of a coated vane.

Keywords: turbine vane; thermal barrier coating; film cooling; overall cooling effectiveness

1. Introduction

Because of the continuing demand for the increment of thermal efficiency and the decline of fuel consumption, the inlet temperature of gas turbines has far exceeded the normal material temperature limits of the vane over the previous century [1,2]. Thus, multiple cooling and thermal protection techniques have applied to ensure gas turbine working within safety margins, which include internal cooling and film cooling, as well as thermal barrier coatings (TBCs) [3,4].

The shape and location of internal cooling channels, as well as temperature and mass flux of the coolant consumption influence cooling performances and temperature gradient of the internal cooled vane [3–5]. The location and shape optimization of cooling channels, as well as enhanced heat transfer techniques, such as the introduction of turbulators and pinbanks within the internal cooling channels, are the main ways to improve internal heat transfer [6,7]. Because of the complex three-dimensional unsteady flow caused by the mixing of the coolant ejections and external hot gas, the prediction of film cooling performance is much more difficult than that of internal cooling [8]. Coolant and mainstream conditions, as well as airfoil geometry, influence the film cooling performance [8–10]. Because of the limited gains of the further improvement of the internal cooling and film cooling techniques, TBCs with internal cooling and film cooling techniques have applied in advanced gas turbine vane designs over the previous century [2].

Recently, the method of three-dimensional conjugate heat transfer method (3D CHT), which conjugately calculates both fluid domain and solid body, have applied in predicting the heat transfer, thermal load and cooling performances for a specific turbine vane or blade [11,12]. However, most of the previous works focused on the uncoated vane with internal cooling or film cooling. For the coated vane, the use of the CHT method still faces many troubles caused by the huge difference between coatings and vane, which result in many difficulties in geometric modeling, meshing and simulation [13–15]. For the coated vane with internal cooling only, some researchers studied the coating thickness and thermal conductivity of an internally cooled vane coated with one layer of coating with the 3D CHT method [12–20]. Bohn et al. [12] studied the combine influences of coating and internal cooling on the aerodynamic and thermal stresses of the NASA Mark II guide vane with 3D CHT method. Their work showed that the maximum drop of temperature appeared in the strong shock area on the suction side (SS), while the minimum value occurred on the trailing edge (TE). The decrease of the coolant inside the internal cooling channels exerted a greater influence on the thermal stresses in the blade material than the coating itself [12]. Liu et al. [13] studied the coating insulation of an internally cooled vane coated with multilayered TBCs. Their work showed that inlet flow condition exerted a greater influence on the coating insulation [13]. Prasert et al. [14] studied the influence of turbulence intensity on the overall cooling performances of an internally cooled vane coated with a constant thickness of 0.03556 cm of ZrO_2. Their work showed that the increment of turbulence intensity had smaller influence on decreasing the average temperature [14]. For the coated vane with film cooling, the geometric modeling and meshing is much more difficult than that of the internal cooled vane, especially for the vane with multilayered TBCs. Prasert et al. [15], Davidson et al. [16] have made good efforts to build the film cooled vane coated with one layer of coating. However, few studies paid attention to the film cooled vane with multilayers of TBCs. TBCs normally consist of the substrate (SUB), top coating (TC), thermally grown oxide (TGO) and bond coating (BC) [13]. The material properties and thermal behaviors are different between layers and vane structure [13]. Thus, building the precise geometry of multilayered TBCs for a specific film cooled vane is still necessary for studying the heat transfer, thermal load, and cooling performances, as well as the TBCs stresses of a coated vane.

Nowadays, TBCs with a film cooling technique have been widely applied in advanced gas turbine vane designs [15]. From the studies that have been performed for the cooling performances and temperature gradient of the film cooled vane or blade, more attention is placed on the uncoated vane, and few studies paid attention to the coated vane. In current study, the precise geometry of film cooled C3X guide vane with layers of TC, TOG and BC are generated by commercial software ANSYS ICEM CFD. The performance of various film cooling ejections on the cooling performances and temperature distributions of the C3X vane with and without the inclusion of external multilayered layers of TBCs have been studied to provide reference for the design of coated vane or blade with film and internal cooling.

2. Geometry and Mesh

Figure 1 shows the schematic diagram of thermal properties of the uncoated vane and coated vane. To explore the influences of the coatings, the thicknesses of BC, TGO and TC layers in this work are set as 150, 10, and 300 μm, respectively. In this work, mainstream gas adopts ideal gas. The specific heat and thermal conductivity coefficient of gas are shown in Table 1. The vane material is 310 stainless steel with a constant density and a constant-pressure specific heat capacity of 8030 kg/m^3 and 502 J/(kg·K), respectively. The thickness and material properties of BC, TGO, and TC are based on the coated Mark II guide vane provided by Liu et al. [13], with the same vane height and similar configuration. The thermal conductivity of BC, TGO, and TC are 4.3–16.1, 25.2, and 1.05 W·m^{-1}·K^{-1} under the temperature between 298–1273 K. Other important material properties of TBCs are shown in Table 1 [13,17,18]. The definition of thermal parameters is illustrated in Equations (1)–(5) [15].

(1) Overall cooling effectiveness of the uncoated vane (φ):

$$\phi = \frac{T_\infty - T}{T_\infty - T_c} \tag{1}$$

(2) Overall cooling effectiveness of the coated vane (φ_{TBC}):

$$\phi_{TBC} = \frac{T_\infty - T_{TBC}}{T_\infty - T_c} \tag{2}$$

(3) Overall cooling effectiveness increment due to TBCs ($\Delta\varphi$):

$$\Delta\phi = \left(\frac{\phi_{TBC} - \phi}{\phi}\right) \times 100\% \tag{3}$$

(4) Relative change of surface temperature distribution due to TBCs ($\Delta T'$):

$$\Delta T' = \frac{T' - T}{T_{ref}}, T_{ref} = 701\text{K} \tag{4}$$

(5) Reduction of the substrate temperature due to TBCs (ΔT_{TBC}):

$$\Delta T_{TBC} = \frac{T' - T_{TBC}}{T_{ref}}, T_{ref} = 701\text{K} \tag{5}$$

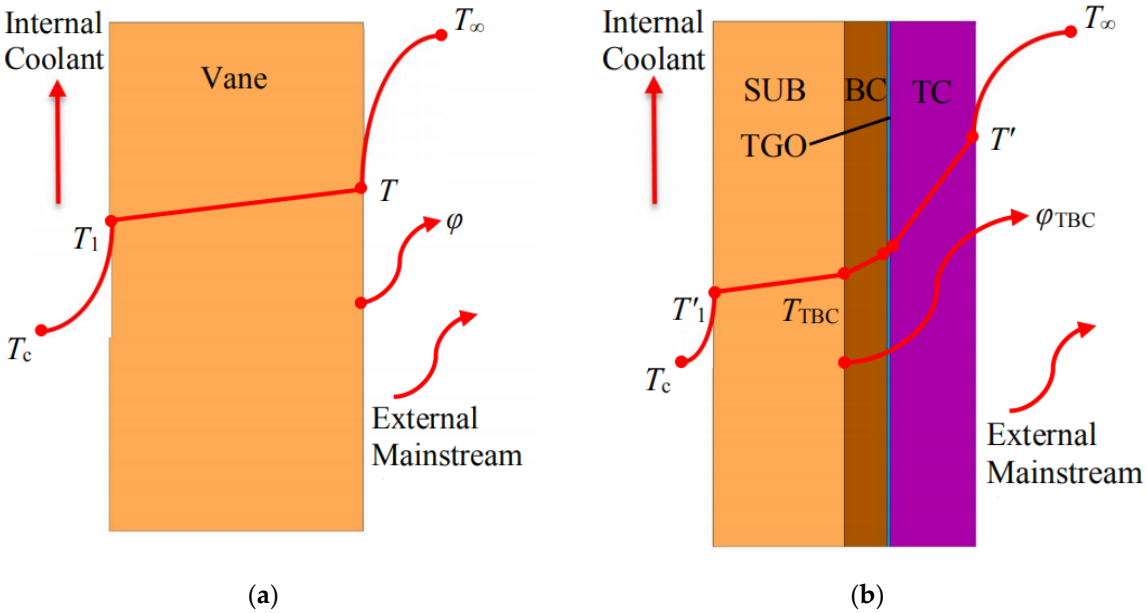


Figure 1. Thermal parameters definition. (**a**) uncoated vane; (**b**) coated vane.

Table 1. Material properties [13,17,18].

Material	Temperature	Density	Specific Heat	Thermal Conductivity
GAS	298–1273 K	Ideal gas	$C_p = 938 + 0.196\ T$	$k_f = 0.0102 + 5.8 \times 10^{-5}\ T$
SUB	298–1273 K	8030 kg/m^3	502 J/kg·K	$k(T) = 0.0115\ T + 9.9105$
BC	298–1273 K	7320 kg/m^3	501–764 J/kg·K	4.3–16.1 W/m·K
TGO	298–1273 K	3978 kg/m^3	857 J/kg·K	25.2 W/m·K
TC	298–1273 K	5650 kg/m^3	483 J/kg·K	1.05 W/m·K

Despite great progress in the calculation accuracy of the CHT method, the numerical results must be confirmed by the experimental data, which is less common in open literature [16]. The film cooled C3X vane reported by Hylton et al. [17,18] is a stainless-steel nozzle guide vane (NGV) with no twist; the height and true chord of the vane are 7.62 cm and 14.493 cm, respectively [18]. The forward portion of the vane consists of three coolant plenums which feed coolant to 152 film cooling holes mounted on the leading edge (LE), pressure side (PS) and suction side (SS)—see Figure 2a [18]. There are 5, 2, and 2 rows of film cooling holes mounted on the LE, PS, and SS of the vane—see Figure 3. Ten radial cooling holes are installed along the axial of the aft portion of the vane. The two parts mentioned above are split by a thermal barrier in this work—see Figure 2a [20]. The calculation model is a three-vane cascade which includes an internal cooling air domain and three vane structures, as well as the external mainstream domain, which extends up to 1.5 C_{ax} upstream and 2 C_{ax} downstream of the vane—see Figure 2b. The numerical meshes are generated by commercial software ANSYS ICEM CFD. Both the fluid and the solid domain are meshed with unstructured mesh. For the solid domain, the aft portion of the vane is meshed with unstructured hexahedral mesh, while the forward portion uses unstructured algorithm mesh. To improve computational accuracy of boundary layer flows, an O-grid scheme with multilayer of prism or unstructured hexahedral grids is applied to the fluid domain near the vane surface. Three mesh models are used to assure grid independence. The total number of grids for coarse mesh, medium mesh and fine mesh are 10,132,351, 15,358,563 and 20,879,375, respectively. The computational grids for the medium mesh model are demonstrated in Figure 3. For the medium mesh model, there are at least twenty points along the peripheral direction of the film cooling holes, and forty points along the radial cooling channels. The value of $y+$ of the grids adjacent to the solid wall is less than 2. Overall grid in the external fluid domain is about 10.7 million elements, and the grid in SUB, BC layer, TGO layer and TC layer for the coated vane mounted in the center of computational domain are about 0.21, 0.53, 0.18, and 1.05 million, respectively.

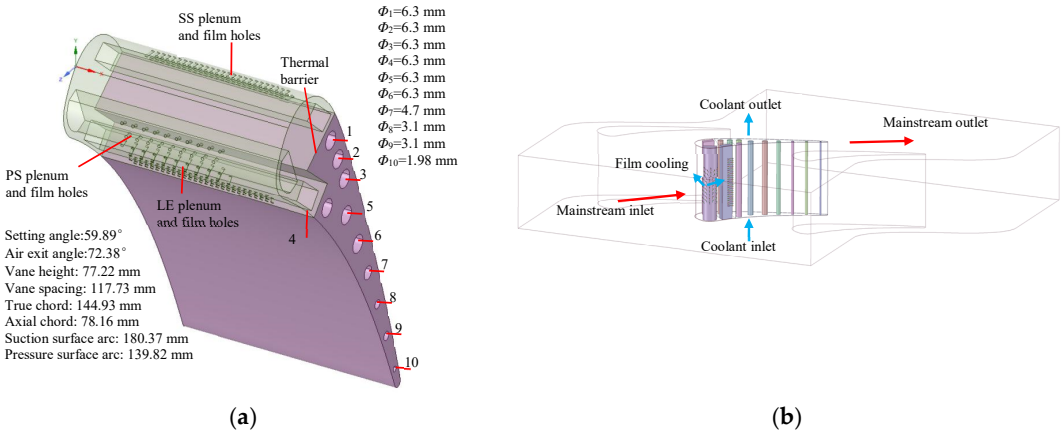


Figure 2. Vane structure and computational domain. (**a**) vane structure, (**b**) computational domain.

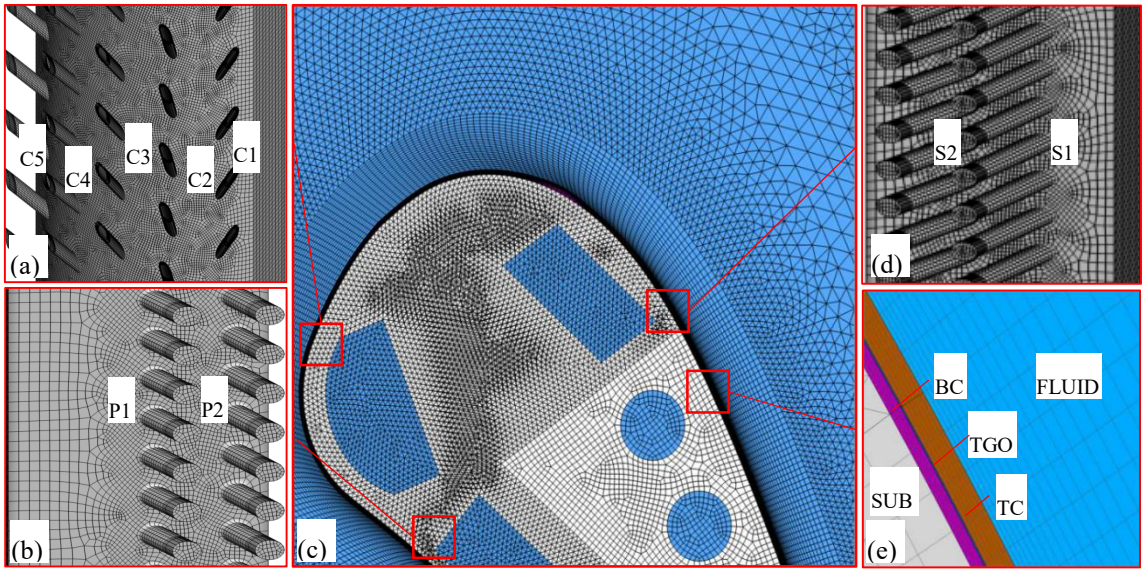


Figure 3. Computational grids. (**a**) leading edge film cooling holes, (**b**) pressure side film cooling holes, (**c**) computational grids, (**d**) suction side film cooling holes, (**e**) multilayered thermal barrier coatings (TBCs).

Numerical simulations carried out in this work were based on the experiment Run 44,344 provided by Hylton et al. [17,18]. For the inlet of hot gas path, total pressure, total temperature and turbulence intensity are 285.13 kPa, 701 K and 6.5%—see Table 2 [17,18]. The mass flow rates of LE, PS and SS coolant plenums are 0.638×10^{-2}, 0.752×10^{-2}, and 0.134×10^{-1} kg/s, with inlet total temperatures of 602.86, 581.83, and 595.85 K, respectively [17,18]. The turbulence intensity is set as 5% for the inlet of coolant plenums [17,18]. Boundary conditions of ten radial cooling holes are consistent with those provided in Ke et al. [19] and Jiang et al. [20]. Finally, boundary conditions of coated vane are identical with the uncoated vane. In order to estimate the temperature distributions of the C3X vane and the insulation characteristics of TBCs, steady state simulations by means of coupling of a CFD calculation with thermal conduction analysis are developed with the commercial code ANSYS FLUENT. The Reynolds averaged continuity, momentum, and the energy equations, along with the *k-kl-ω* turbulence model, are solved in the fluid domains. In the solid domain, only the energy equation is solved on the basis of Fourier's law [14,15]. To improve computational accuracy, the normalized residuals of continuity and energy equations are set as 10^{-3} and 10^{-6}, respectively. The mass flow error between the inlet and exit of the computational domain is less than 0.1%.

Table 2. Boundary conditions [17,18].

Boundary	Value
Inlet total pressure	285.13 kPa
Inlet total temperature	701 K
Inlet turbulence intensity	6.5%
Outlet static pressure	170.42 kPa
Mate flow rates of leading edge coolant plenum	0.638×10^{-2} kg/s
Temperature of leading edge coolant plenum	602.86 K
Mate flow rates of pressure side coolant plenum	0.752×10^{-2} kg/s
Temperature of pressure side coolant plenum	581.83 K
Mate flow rates of suction side coolant plenum	0.134×10^{-1} kg/s
Temperature of suction side coolant plenum	595.85 K
Inlet turbulence intensity of coolant plenums	5%

Figure 4 shows the comparisons between numerical results and experimental data, at the midspan (z = 0 mm). The references total pressure and static temperature are 285.13 kPa and 701 K, respectively [17,18]. Change rules of the total pressure and static temperature show the same trend for different mesh models, and the medium mesh model is the proper choice with enough computational accuracy and efficiency. For dimensionless total pressure distribution, calculated values are in good agreement with the experimental data from Hylton et al. [17,18], although the calculated values are slightly larger in the area between $0.25 < x/C_{ax} < 0.50$, with maximum deviations at about 5%. For static temperature distribution, the calculated value of static temperature is also in good agreement with the experimental data, with maximum deviations less than 5%. In summary, the *k-kl-ω* turbulence model and simulation strategy applied in this work can accurately predict the change trend of pressure and temperature distributions on the vane surface.

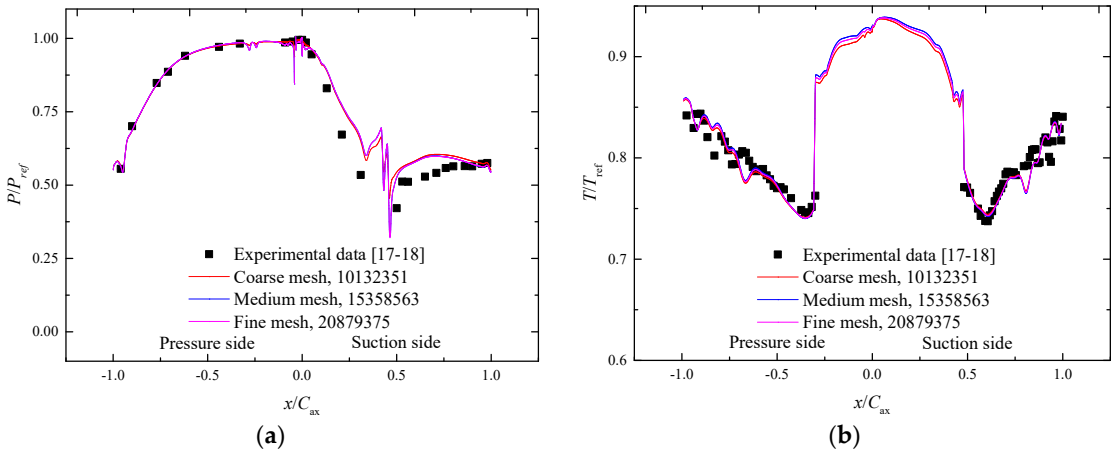


Figure 4. Comparisons between numerical results and experimental data at the midspan (z = 0 mm). (**a**) pressure comparison (P_{ref} = 285.13 kPa), (**b**) temperature comparison (T_{ref} = 701 K).

3. Discussion

3.1. Influence of Film Cooling on the External Surface Temperature Distribution

Figure 5; Figure 6 show the comparisons of dimensionless static temperature and streamlines on the external surface of the uncoated vane, for different cases. For an uncoated vane without film, surface temperature keeps high value on the PS of forward portion. In contrast to this, strong acceleration of external mainstream causes quickly decline of surface temperature on the SS. Further along the vane surface, a local minimum appears between two alongside radial cooling channels, and a local maximum close to a radial channel. Finally, temperature of the hub is much lower than that of the tip, because of the heating of coolant along the radial cooling channels. For uncoated vane with LE film, coolant ejections exhausted from the LE thrust the boundary layer and reattach on the downstream of vane surface. Thus, coolant ejections cannot cover the regions close to the exits of the LE film cooling holes, especially for ejections from the C3 row—see Figure 6. Meanwhile, coolant ejections exhausted from the rows C1, C2, and C3 inject toward to the PS, while the rows C4 and C5 toward to the SS. On the aft portion of the vane, significant radial flow in the coolant ejections improve the coverage of film cooling and thus decrease the temperature on the regions close to the tip. In contrast to this, radial flow weakens on the SS.

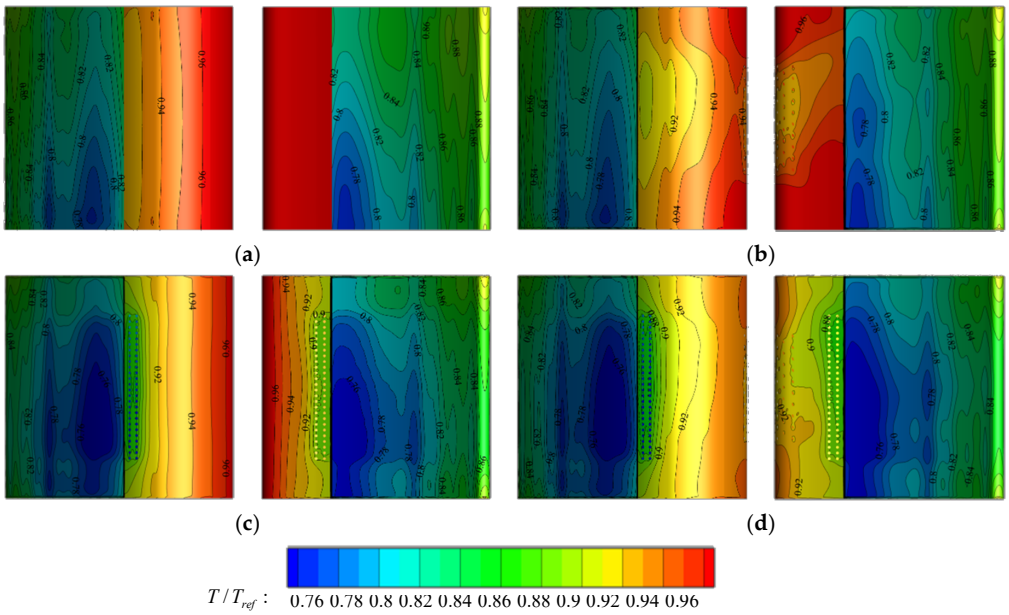


Figure 5. Temperature comparisons for different cases (T_{ref} = 701 K). (**a**) uncoated vane without film, (**b**) uncoated vane with LE film, (**c**) uncoated vane with downstream film, (**d**) uncoated vane with LE and downstream film.

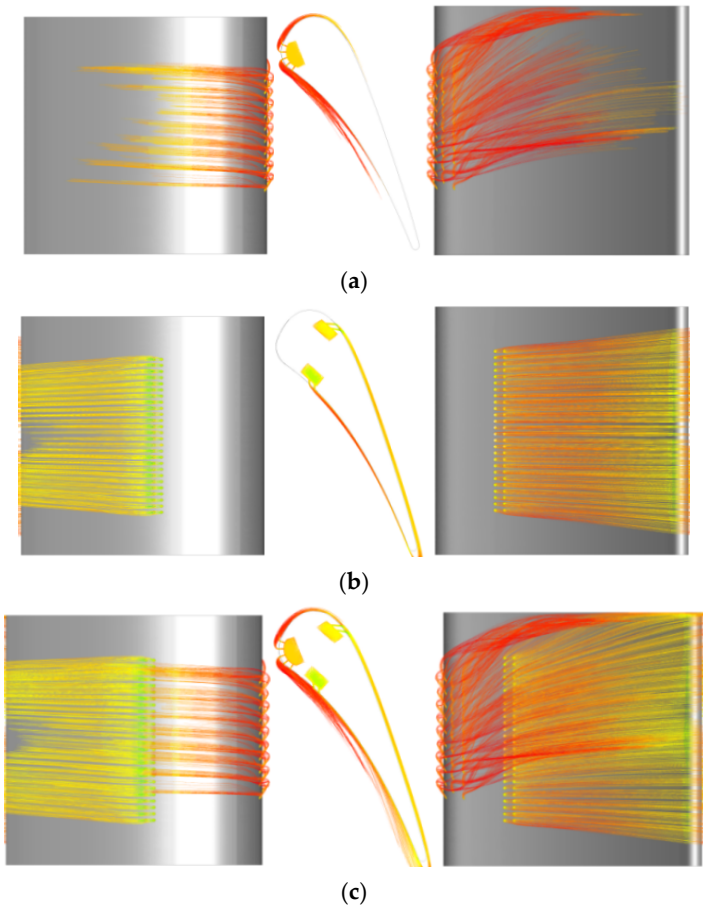


Figure 6. Streamlines distribution comparisons for different cases. (**a**) uncoated vane with LE film, (**b**) uncoated vane with downstream film, (**c**) uncoated vane with LE and downstream film.

For uncoated vane with downstream film, shorter reattach distances of coolant ejections from downstream film cooling holes improve the coverage of film cooling over the vane surface. Meanwhile, significant radial flow in the coolant ejections from PS film cooling holes extend the coverage of film cooling and thus decrease the temperature on the hub and tip of the TE. In contrast to this, radial flow from SS film cooling holes weakens on the SS. For uncoated vane with LE and downstream film, most of the ejections exhausted from LE lift off and reattach on the far downstream of vane surface which caused by the influence of downstream coolant ejections, see in Figure 6. On the SS, coolants from LE reattach and blend with the downstream coolant ejections and hot gas on the aft portion. Under the influence of ejections from LE, ejections from PS film cooling holes also show significant radial flow, which extends the coverage of film cooling and thus decreases the temperature on the tip of TE. However, radial flow of coolant ejections both from the LE and downstream film cooling holes weaken on the SS. This result suggests that multiple cooling and thermal protection techniques including internal cooling and TBCs are necessary on the TE of the SS.

Figure 7 shows the comparisons of the dimensionless temperature distributions along the external wall of the uncoated vane at cutting planes of $z = -19.3$ mm, $z = 0$ mm and $z = 19.3$ mm, for different cases. For an uncoated vane without film, a local maximum of temperature appears on the regions close to the stagnation line, which is about 686 K, at all cutting planes. Temperature on the PS is higher than the SS of the forward portion. On the PS of aft portion, a local minimum appears in the area around $x/C_{ax} = -0.36$, which is near the radial channel of No. 4. Further along the TE, the second minimum appears around $x/C_{ax} = -0.67$, which is near the radial channel of No. 7. On the SS, the temperature distribution is similar to that of the PS, where a local minimum appears in the area around $x/C_{ax} = 0.6$, while the second appears around $x/C_{ax} = 0.8$. For uncoated vane with LE film, the decreasing amplitude of temperature on the SS is much smaller than that on the PS of the aft portion, especially at a cutting plane of $z = 19.3$ mm. In comparison with the no film case, temperature decline is about 15.6 K at $x/C_{ax} = -0.36$; close to the radial channel of No. 4 on the PS. On the SS, the value is decreased to 6.0 K at $x/C_{ax} = 0.6$, near the same radial channel. This result shows that, coolant ejections keep their 3D turbulent flow characteristics and thus provide more effective coverage of film cooling on the PS.

For an uncoated vane with downstream film, the improved the convective heat transfer of coolant with the wall of coolant plenums leads to a further decline in temperature on the forward portion of the vane. In comparison with the no film case, temperature decline is about 6 K at the stagnation point of the midspan ($z = 0$ mm). For an uncoated vane with LE and downstream film, surface temperature is higher than that of the downstream film case on the aft portion, at a cutting plane of $z = -19.3$ mm. In contrast to this, lower surface temperatures appear at other cutting planes. This result suggests that the significant radial flow ingredient of the LE coolant ejections improves the film cooling coverage and thus decreases the temperature near the tip of the vane. In contrast to this, film cooling coverage weakens near the hub, which declines the cooling performances on this region. In comparison with the no film case, introduction of the coolant ejections from LE exert larger influence on the temperature decline for the LE film case. Under the influence of the LE film cooling, temperature decline is about 12.1 K at $x/C_{ax} = -0.36$ of the midspan. In comparison with the downstream film case, the influence of LE film is much smaller for the LE and downstream film case. Temperature decline is only about 3.4 K, at the same position. This result suggests that the interconnected influence between various coolant ejections leads to part of the coolant ejections lifting off the surface of the vane and thus offseting the cooling performances on those regions.

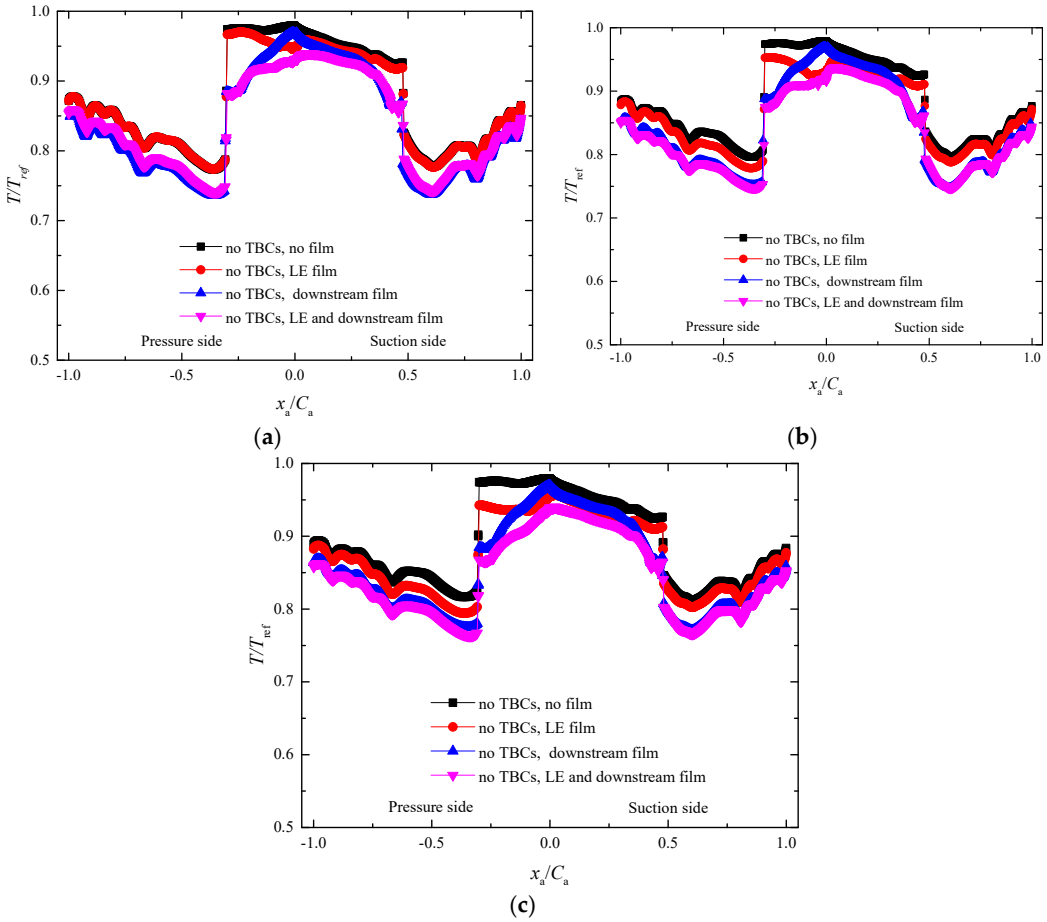


Figure 7. Surface temperature distribution comparisons for different cases. (**a**) $z = -19.3$ mm, (**b**) $z = 0$ mm, (**c**) $z = 19.3$ mm.

3.2. Influence of Film Cooling on the Relative Change of Temperature Outside the TBCs

Figure 8 shows the comparisons of relative temperature change outside the TBCs, for different cases. Positive value means an increase in surface temperature. For the coated vane, the largest temperature gradient appears in the TBCs because of their lower thermal conductivity. Thus, in most parts of the vane, although the surface temperature increases outside the TBCs, the temperature of substrate metal is still lower than that of the uncoated vane. For the coated vane without film, surface temperature increases in most part of the coated vane. In contract to this, regions with negative value on the SS appear close to the SS coolant plenum. On the aft portion, larger relative temperature change appears on the regions near the radial channel and the value of the hub is much larger than that of the tip. For the coated vane with LE film, regions with negative value appear on the PS of the forward portion, where they are away from the LE coolant plenum and effectively covered by the LE film cooling. Meanwhile, regions with negative value on the SS appear in the same position as that of the no film case. For coated vane with downstream film, new regions with negative value appear close to the downstream the PS and SS film cooling holes. For coated vane with LE and downstream film, temperature change distribution on the forward portion is similar to that of the LE film case. However, regions decline on both sides of the forward portion, which is because the internal cooling improvement was caused by introduction of the downstream film coolant. For the aft portion, smaller values appear on the regions under the effective coverage of film cooling. In contrast to this, a larger value appears on the regions close to the hub with sufficiency internal cooling.

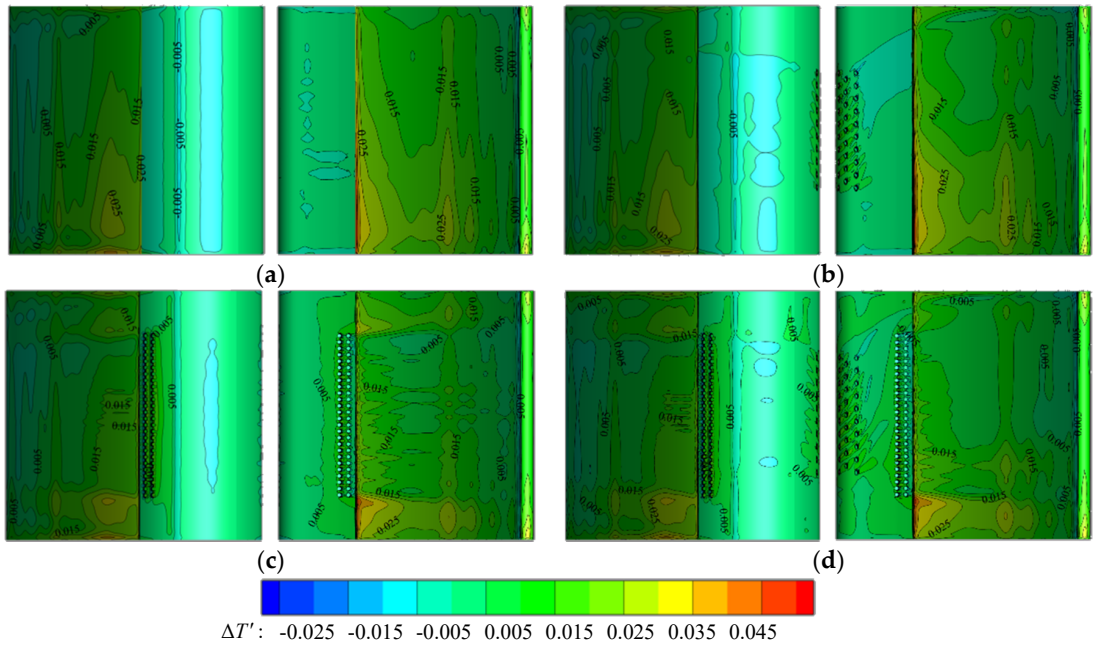


Figure 8. Surface temperature comparisons for different cases. (**a**) coated vane without film, (**b**) coated vane with LE film, (**c**) coated vane with downstream film, (**d**) coated vane with LE and downstream film.

Figure 9 shows the comparisons of temperature distributions along lines from the free stream of the PS to the SS at the midspan, for different cases. Figure 10 shows the relative temperature changes along external wall at cutting planes of $z = -19.3$ mm, $z = 0$ mm and $z = 19.3$ mm, for different cases. For the uncoated and coated vane without film, higher surface temperature level appears on the PS of the forward portion. The influence of TBCs on relative temperature change is smaller on this region. On the SS, there is a variation of relative temperature change in the area between $0.13 < x/C_{ax} < 0.48$. In this area, a local minimum appears at $x/C_{ax} \approx 0.33$, which is about −4 K, for all cutting planes. For coated vane with LE film, relative temperature change close to the LE coolant plenum is always larger than other regions of forward portion, especially on the midspan where the LE film cooling holes are mounted. In comparison with the no film case, smaller values appear in the areas between $-0.3 < x/C_{ax} < -0.21$ on the PS and $0.23 < x/C_{ax} < 0.34$ on the SS. At cutting plane of $z = 19.3$ mm, negative values appear in the area between $-0.11 < x/C_{ax} < -0.08$ on the PS. This result suggests that internal cooling improvement caused by coolant introduction leads larger relative temperature change on the regions close to coolant plenums and film cooling holes. In contrast to this, coverage of film cooling declines the relative temperature change outside the TBCs. For coated vane with downstream film, regions with negative values appear on the downstream the PS and SS film cooling holes. For coated vane with LE and downstream film, the value of relative temperature change on the forward portion is larger than other cases at cutting plane $z = -19.3$ mm, which is because of the internal cooling improvement. In comparison with the downstream film case, smaller values of relative temperature change appear close to the upstream of downstream plenums at the cutting plane of $z = 19.3$ mm. For the aft portion of the vane, temperature of substrate metal is lower than external mainstream, see Figure 9. The improved film cooling coverage declines the relative temperature change on the aft portion of the vane, for all cutting planes.

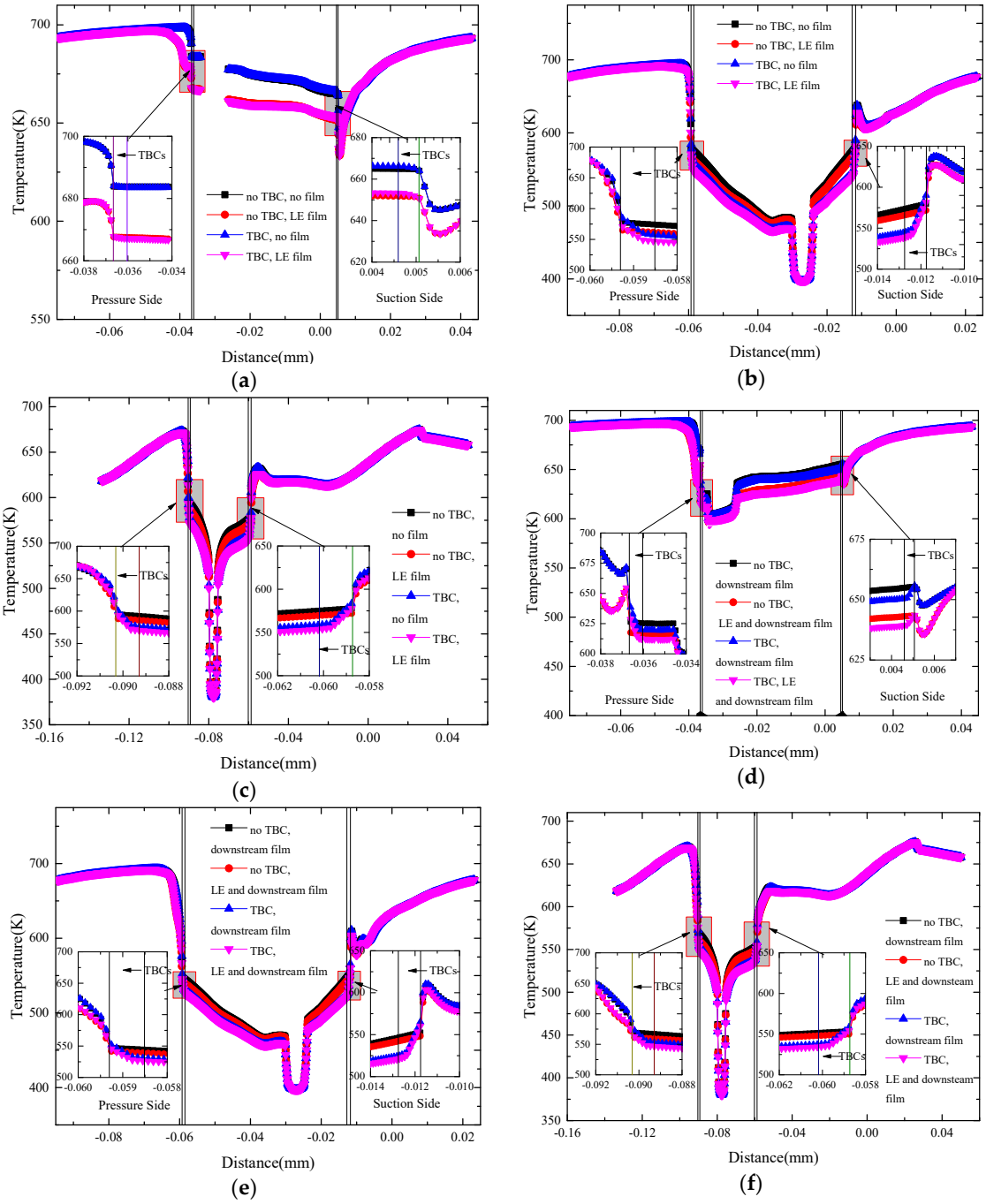


Figure 9. Temperature distribution comparisons for different cases. (**a**) x = 0.25 C_{ax}, (**b**) x = 0.5 C_{ax}, (**c**) x = 0.75 C_{ax}, (**d**) x = 0.25 C_{ax}, (**e**) x = 0.5 C_{ax}, (**f**) x = 0.75 C_{ax}.

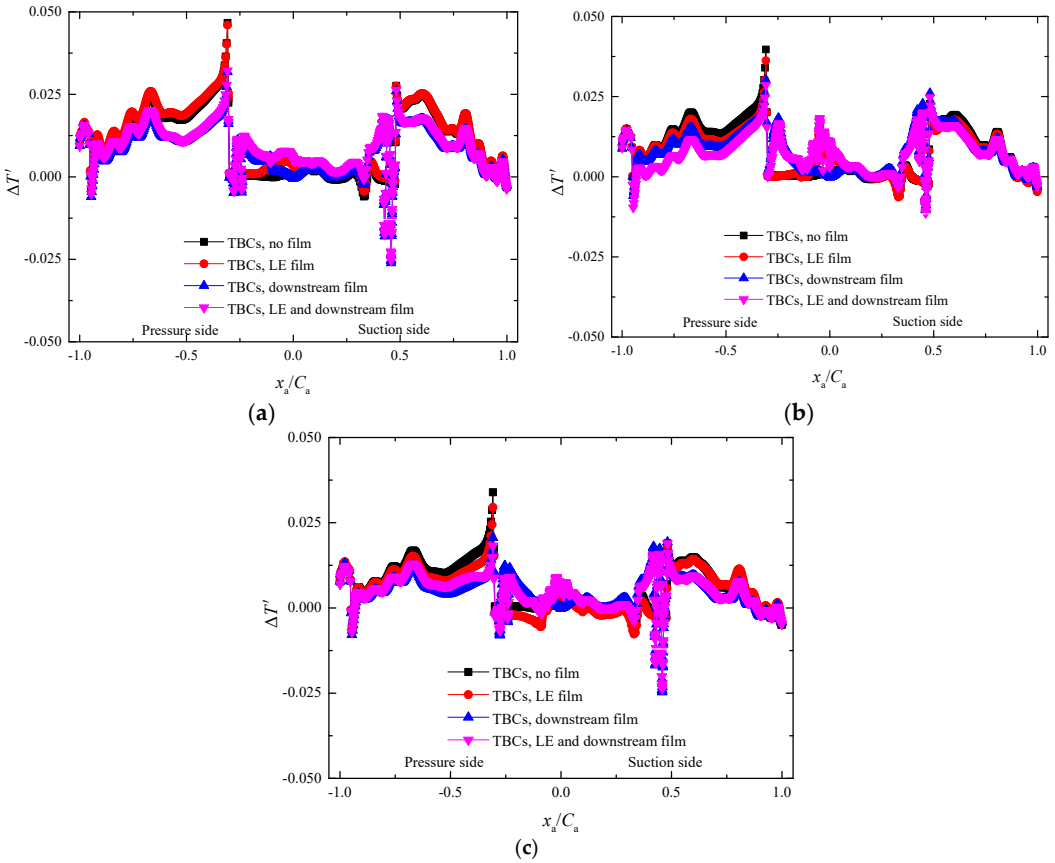


Figure 10. Relative temperature change comparisons for different cases. (**a**) $z = -19.3$ mm, (**b**) $z = 0$ mm, (**c**) $z = 19.3$ mm.

3.3. Influence of Film Cooling on the Temperature Reduction Due to TBCs

Figure 11 shows the comparisons of substrate temperature distribution, for different cases. As mentioned above, the largest temperature gradient appears in the TBCs. Thus, temperature substrate surface is lower than of the uncoated vane in the most part of the vane. For coated vane without film, substrate temperature of the PS is higher than that of the SS on the forward portion of the vane. Further along the vane surface, a local minimum appears close to a radial cooling channel, and the temperature level at the tip is higher than that of the hub. For coated vane with LE film, substrate temperature decreases on the regions covered by the LE film cooling on the both side of the forward portion. However, higher temperature appears close to the hub and the tip of forward portion, where it is unprotected by film cooling. For coated vane with downstream film, a local maximum appears near the stagnation line. Further along the vane surface of the forward portion, the substrate temperature decreases on both sides of the vane, especially on the regions close to the downstream film cooling holes. For the coated vane with LE and downstream film, the improvement of internal cooling cause strong decline of temperature on the forward portion of the vane, especially on the regions close to the hub and the tip of the forward portion. For the aft portion, a local minimum appears between two alongside radial cooling channels, and a local maximum close to a radial channel. Meanwhile, under the influence of TBCs, temperature distribution is more uniform over the surface of substrate, for different cases. Finally, the improved film cooling coverage leads to lower substrate temperature on the aft portion of the vane.

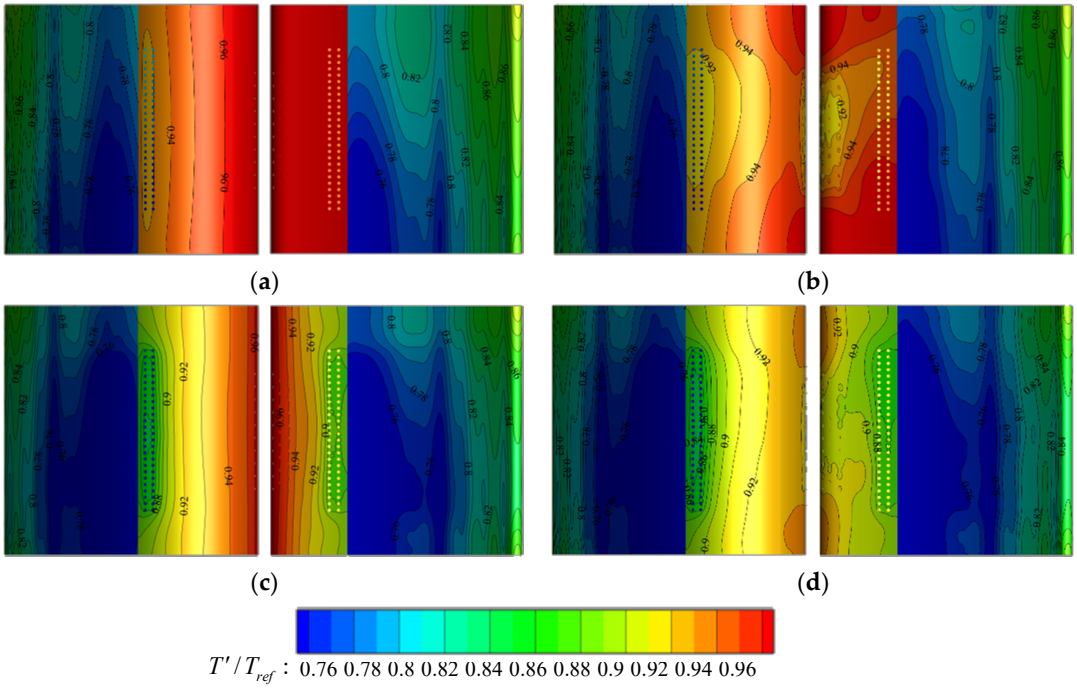


Figure 11. Substrate temperature comparisons for different cases. (T_{ref} = 701 K). (**a**) uncoated vane without film, (**b**) uncoated vane with LE film, (**c**) uncoated vane with downstream film, (**d**) uncoated vane with LE and downstream film.

Figure 12 shows the comparisons of temperature decline in the substrate material at cutting planes of z = −19.3 mm, z = 0 mm and z = 19.3 mm, for different cases. Positive value means that the temperature of the substrate surface is lower than that of the coatings surface. For coated vane without film, TBCs on the PS is more effective than on the SS and regions, with negative values appearing in the area between $0.13 < x/C_{ax} < 0.48$, for all cutting planes. In this area, a local minimum appears at $x/C_{ax} \approx 0.33$, which is equal to −3.2 K at the midspan. This result suggests that, even without film cooling, the temperature of external hot gas can still be lower than that of the substrate metal. The lower temperature is caused by strong acceleration of mainstream from the stagnation line of the SS. In this area, TBCs hamper the heat flux transfer from substrate metal into the external mainstream. Thus, without film cooling, effectively internal cooling inside the vane is the premise of overall cooling effectiveness increment for coated vane. For coated vane with LE film, the temperature decline close to LE coolant plenum is always larger than other regions on forward portion of the vane, especially at the midspan where the LE film cooling holes mounted. As mentioned before, there are no film holes mounted on the LE of the cutting plane of z = −19.3 mm and z = −19.3 mm. At cutting plane of z = −19.3 mm, TBCs are more effective than that of the no film case on the forward portion of the vane, which is because of the internal cooling improvement on this plane. At a cutting plane of z = 19.3 mm, negative values appear on the PS of forward portion, as well as the regions at the same position of the no film case on the SS. In this area, a local minimum appears around x/C_{ax} = 0.33, which is about −4 K at this plane. This result suggests that internal cooling improvement caused by coolant introduction increase the temperature gradient of TBCs on the regions close to coolant plenums and film cooling holes. However, the influence of TBCs addition goes down, and even shows negative roles on the regions away from coolant plenums and under the effective coverage of film cooling. For coated vane with LE and downstream film, smaller values appear on the regions close to the upstream of the PS and SS plenum at the cutting plane of midspan and z = 19.3 mm, in comparison with the downstream film case. On the aft portion of the vane, the improved film cooling coverage leads to a smaller temperature gradient inside the TBCs. As mentioned before, the forward and aft portion of the vane is split by a

thermal barrier. Introduction of film cooling on the forward portion has no influence on the internal cooling of aft portion. Thus, the improved film cooling coverage declines the thermal insulation effect of TBCs on the aft portion of the vane.

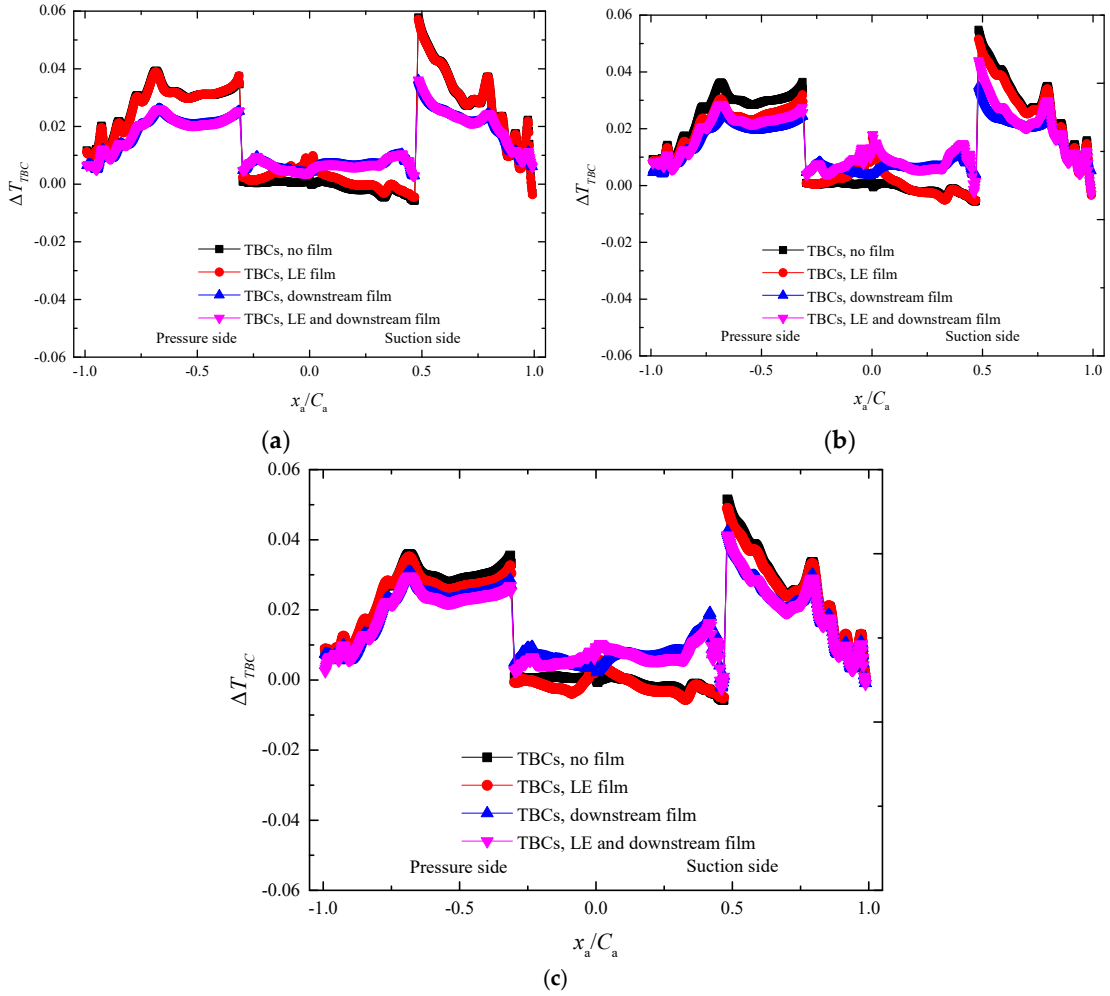


Figure 12. Temperature reduction distribution comparisons for different cases. (**a**) z = −19.3 mm, (**b**) z = 0 mm, (**c**) z = 19.3 mm.

3.4. Influence of Film Cooling on the Increment of Overall Cooling Effectiveness

Figure 13 shows the comparisons of the overall cooling effectiveness increment due to TBCs, for different cases. For coated vane without film, the overall cooling effectiveness due to TBCs decreases on the SS of the forward portion, especially on the regions close to the SS coolant plenum. On the aft portion, a local maximum appears on the regions close to the radial channel, and the increment of overall cooling effectiveness on the tip is larger than that of the hub. This result suggests that the decline of heat flux hampered by TBCs limits the temperature rise rate of the coolant inside the cooling channels which is helpful to improve the overall cooling effectiveness on the tip of the coated vane. For coated vane with LE film, the overall cooling effectiveness due to TBCs increases on the hub and tip of the LE where close to the LE plenum, and not under the coverage of film cooling. On the PS of the forward portion, negative values appear on the regions away from the LE plenum and under coverage of the LE film cooling. On the SS of forward portion, negative values appear at the same position as that of the no film case. For coated vane with downstream film, overall cooling effectiveness increases at most part of the forward portion, except the regions downstream of the PS and SS film cooling holes. For coated vane with LE and downstream film, the increment of overall cooling effectiveness close to

the tip is smaller than that of the downstream film case, because of the influence of the LE film cooling. For the aft portion of the vane, the improved film cooling coverage leads to slighter overall cooling effectiveness increment due to TBCs.

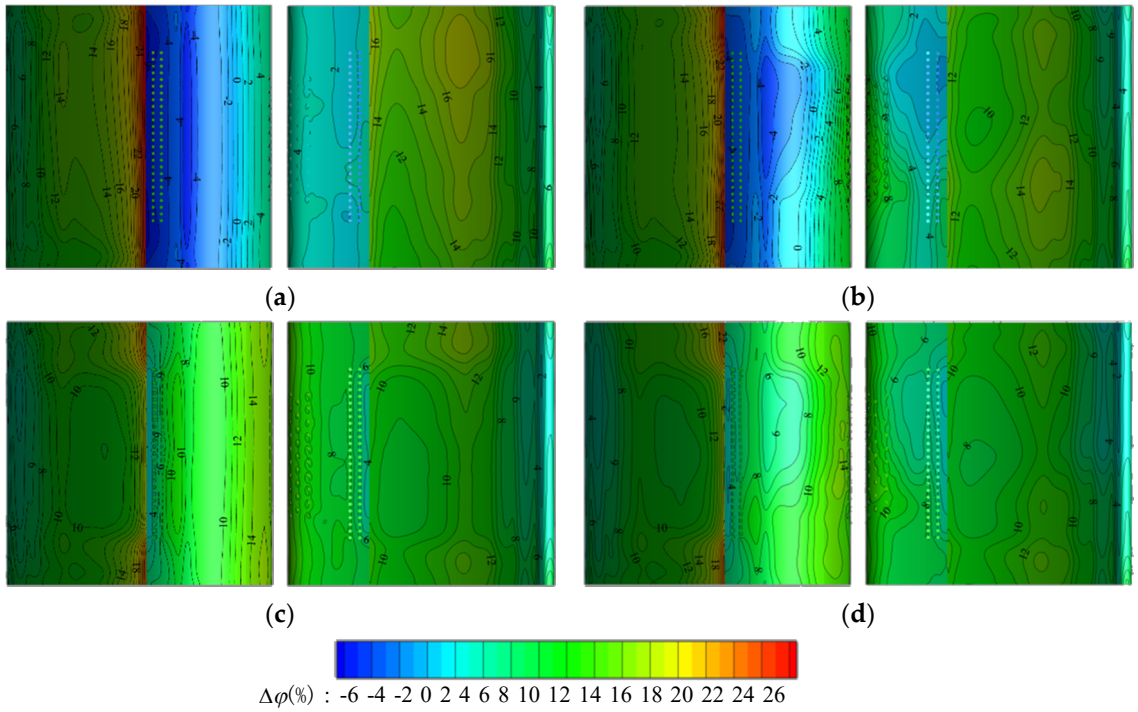


Figure 13. Overall cooling effectiveness comparisons increment for different cases. (**a**) uncoated vane without film, (**b**) uncoated vane with LE film, (**c**) uncoated vane with downstream film, (**d**) uncoated vane with LE and downstream film.

Figure 14 shows the increment of overall cooling effectiveness due to TBCs at cutting planes of $z = -19.3$ mm, $z = 0$ mm and $z = 19.3$ mm, for different cases. For coated vane without film, negative values appear in the area between $0.13 < x/C_{ax} < 0.48$, for all cutting plane. In this area, a local minimum appears around $x/C_{ax} = 0.33$, for all cutting planes. For coated vane with LE film, increment of overall cooling effectiveness close to LE coolant plenum is always larger than the other regions of the forward portion. The local maxima of overall cooling effectiveness increment on forward portion are 9.7%, 10.7% and 8.9%, for cutting plane of $z = -19.3$ mm, $z = 0$ mm and $z = 19.3$ mm, respectively. However, TBCs show negative roles on the regions away from the coolant plenum and directly cooled by the LE film cooling, especially at cutting plane of $z = 19.3$. In comparison with the no film case, smaller values appear in the area between $-0.3 < x/C_{ax} < -0.08$, at cutting plane of $z = 19.3$. This result suggests that the internal cooling improvement caused by coolant introduction leads larger cooling effectiveness inclement due to TBCs on the regions close to coolant plenums and film cooling holes. In contrast to this, coverage of film cooling reduces the heat flux and thus decreases temperature gradients in the TBCs on the regions away from coolant plenums and protected by film cooling. On the regions with insufficient internal cooling, coolant ejections cooling the coating surface directly which decline the cooling effectiveness on those regions, in comparison with the uncoated vane. For coated vane with LE and downstream film, the value is smaller than that of the downstream film cases, especially at cutting plane $z = 19.3$ which is because of the influence of the LE film cooling. Meanwhile, without considering the impact of coolant ejections on the internal cooling of the aft portion, the improved film cooling coverage leads to smaller overall cooling effectiveness increment due to TBCs. Thus, improving the convective heat transfer of coolant with the wall of coolant plenums and film cooling holes is the guarantee of improving the cooling performance of coated vane with film and internal cooling.

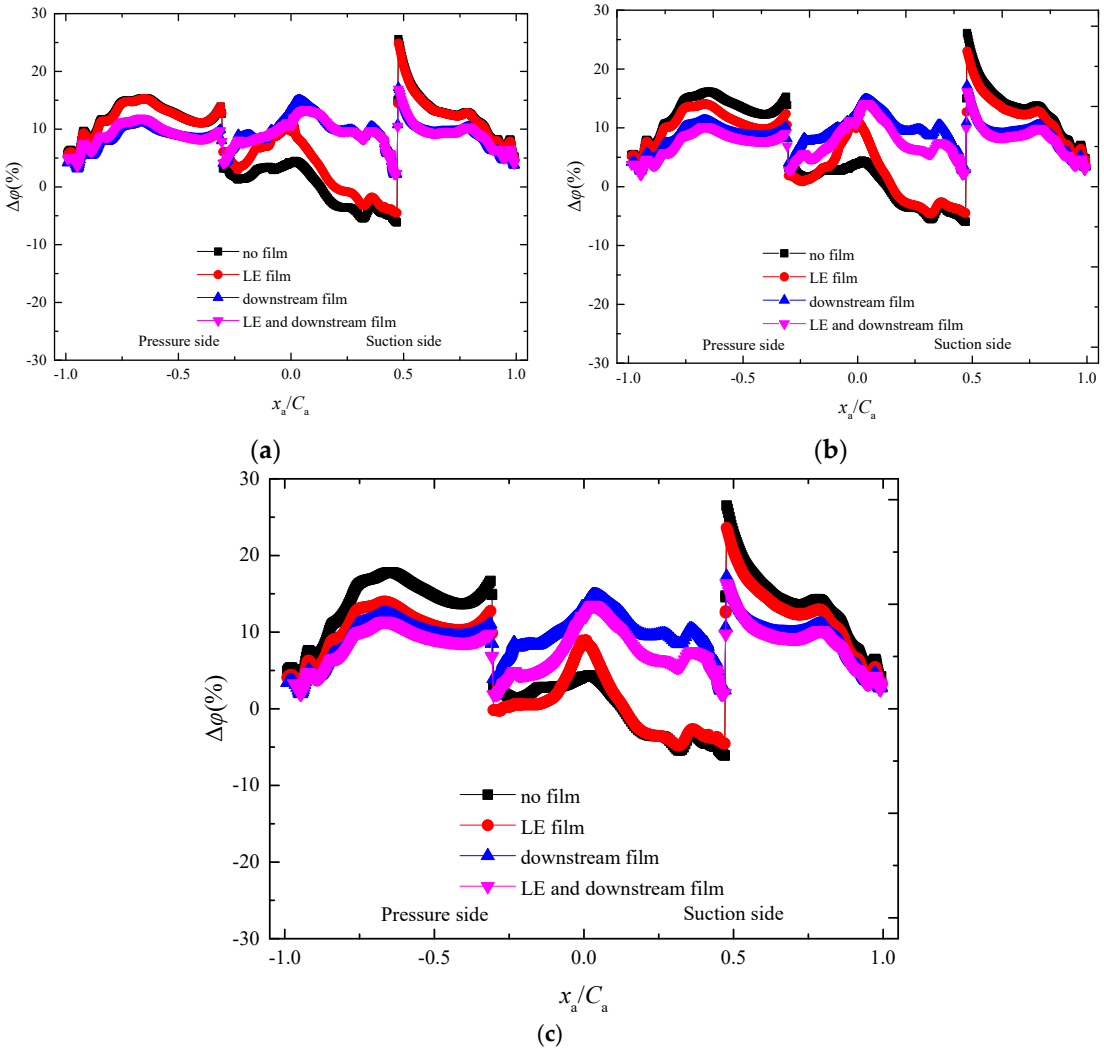


Figure 14. Overall cooling effectiveness increment distribution comparisons for different cases. (**a**) z = −19.3 mm, (**b**) z = 0 mm, (**c**) z = 19.3 mm.

4. Conclusions

This paper studies the combined influences of the film cooling and TBCs on the cooling performances of a coated C3X vane to provide reference for the design of turbine vane or blade. The following conclusions can be drawn:

- Coolant ejections keep their 3D turbulent flow characteristics and thus provide more effective coverage of film cooling on the pressure side (PS). For uncoated vane with LE film, temperature decline is about 15.6 K at x/C_{ax} = −0.36 in comparison with the no film case. On the suction side (SS), the value is decrease to about 6.0 K near the same radial channel.
- The interconnected influence between various coolant ejections leads to a part of coolant ejections lifting off the surface of vane and thus offset the cooling performances on those regions. For the uncoated vane with LE film, temperature decline is about 12.1 K at x/C_{ax} = −0.36 at the midspan, in comparison with the no film case. For uncoated vane with LE and downstream film, temperature decline is only about 3.4 K at the same position in comparison with the downstream film case.
- TBCs show positive and negative roles on the cooling performance increment at the same time for the coated vane, with or without film cooling. For coated vane without film, overall cooling effectiveness decreases in the area between 0.13 < x/C_{ax} < 0.48, with the maximum of about

−5.5%, for all cutting plane. In this area, lower temperature of external hot gas caused by strong acceleration of mainstream from the stagnation line of the suction side (SS).

- Internal cooling improvement caused by coolant introduction leads to larger cooling effectiveness inclement due to TBCs on the regions close to coolant plenums and film cooling holes. However, the influence of TBCs goes down, and even shows negative roles on the regions away from coolant plenums and under effective coverage of film cooling. Thus, improving the convective heat transfer of coolant with the wall of coolant plenums and film cooling holes is the guarantee of improving the cooling performance of the coated vane with film and internal cooling.

Author Contributions: In this paper, L.S. carried out the simulation, and wrote this paper. Z.S. improved the discussions; and Y.L. improved this paper overall. All authors have read and agreed to the published version of the manuscript.

Funding: This research was funded by National Natural Science Foundation of China, grant number 51806184 and Natural Science Foundation of Hunan Province, grant number 2019JJ50590.

Conflicts of Interest: The authors declare no conflict of interest.

Nomenclature

3D	three-dimensional
BC	bond coating
C_{ax}	axial chord(mm)
CHT	conjugate heat transfer
$C_{p,BC}$	specific heat capacity of bond coating (J/kg·K)
$C_{p,f}$	specific heat capacity of fluid (J/kg·K)
$C_{p,SUB}$	specific heat capacity of substrate (J/kg·K)
$C_{p,TC}$	specific heat capacity of top coating (J/kg·K)
$C_{p,TGO}$	specific heat capacity of thermally grown oxide (J/kg·K)
h	heat transfer coefficient, $q/(T_\infty - T_w)$
h_{ref}	reference heat transfer coefficient (1135.6 W/(m^2·K))
k_{BC}	thermal conductivity of bond coating (J/kg·K)
k_f	thermal conductivity of fluid (J/kg·K)
k_{SUB}	thermal conductivity of substrate (J/kg·K)
k_{TC}	thermal conductivity of top coating (J/kg·K)
k_{TGO}	thermal conductivity of thermally grown oxide (J/kg·K)
LE	leading edge
NGV	nozzle guide vane
P	pressure (Pa)
P_{ref}	reference pressure (285.13×10^3 Pa)
PS	pressure side
SS	suction side
SUB	substrate
T	metal surface temperature without TBC (K)
TBCs	thermal barrier coatings
TC	top coating
T_c	inlet temperature of cooling air (K)
TE	trailing edge
TGO	thermally grown oxide
T_{ref}	reference temperature (701 K)
T_{TBC}	metal surface temperature with TBC (K)
T_w	vane local wall temperature (K)
T_∞	inlet temperature of mainstream (K)
T'	surface temperature outside the coating (K)

ΔT_{TBC}	relative reduction of the substrate temperature due to coating
x, y, z	cartesian coordinates(mm)
Greek Symbols	
ρ_{SUB}	density of substrate (kg/m^3)
ρ_{TC}	density of top coating (kg/m^3)
ρ_{TGO}	density of thermally grown oxide (kg/m^3)
ρ_{BC}	density of bond coating (kg/m^3)
φ	overall cooling effectiveness of the uncoated vane
φ_{TBC}	overall cooling effectiveness of the coated vane
$\Delta\varphi$	overall cooling effectiveness increment due to coating (%)

References

1. Huh, M.; Han, J.-C. Recent studies in turbine blade internal cooling. *Heat Transf. Res.* **2010**, *41*, 803–828. [CrossRef]
2. Zhang, J.; Zhu, X.-D.; Huang, Y.; Wang, C.-H. Investigation on film cooling performance from a row of round-to-slot holes on flat plate. *Int. J. Therm. Sci.* **2017**, *118*, 207–225. [CrossRef]
3. Feuerstein, A.; Knapp, J.; Taylor, T.; Ashary, A.; Bolcavage, A.; Hitchman, N. Technical and economical aspects of current thermal barrier coating systems for gas turbine engines by thermal spray and EBPVD: A review. *J. Therm. Spray Technol.* **2008**, *17*, 199–213. [CrossRef]
4. Padture, N.P. Thermal barrier coatings for gas-turbine engine applications. *Science* **2002**, *296*, 280–284. [CrossRef] [PubMed]
5. Singh, P.; Ji, Y.; Ekkad, S.V. Experimental and numerical investigation of heat and fluid flow in a square duct featuring criss-cross rib patterns. *Appl. Therm. Eng.* **2018**, *128*, 415–425. [CrossRef]
6. Wang, L.; Wang, S.; Wen, F.; Zhou, X.; Wang, Z. Effects of continuous wavy ribs on heat transfer and cooling air flow in a square single-pass channel of turbine blade. *Int. J. Heat Mass Transf.* **2018**, *121*, 514–533. [CrossRef]
7. Xie, G.-N.; Liu, X.; Yan, H.; Qin, J. Turbulent flow characteristics and heat transfer enhancement in a square channel with various crescent ribs on one wall. *Int. J. Heat Mass Transf.* **2017**, *115*, 283–295. [CrossRef]
8. Moeini, A.; Zargarabadi, M.R. Genetic algorithm optimization of film cooling effectiveness over a rotating blade. *Int. J. Therm. Sci.* **2018**, *125*, 248–255. [CrossRef]
9. Bunker, R.S. A Review of Shaped Hole Turbine Film-Cooling Technology. *J. Heat Transf.* **2005**, *127*, 441–453. [CrossRef]
10. Dong, P.; Wang, Q.; Guo, Z.; Huang, H.; Feng, G. Conjugate calculation of gas turbine banes cooled with leading edge films. *Chin. J. Aeronaut.* **2009**, *22*, 145–152. [CrossRef]
11. Ekkad, S.V.; Han, J.C. Film Cooling Measurements on Cylindrical Models with Simulated Thermal Barrier Coating Spallation. *J. Thermophys. Heat Transf.* **2000**, *14*, 194–200. [CrossRef]
12. Bohn, D.E.; Tümmers, C. Numerical 3-D Conjugate flow and heat transfer investigation of a transonic convection-cooled thermal barrier coated turbine guide vane with reduced cooling fluid mass flow. In Proceedings of the ASME Turbo Expo 2003, Collocated with the 2003 International Joint Power Generation Conference, Atlanta, GA, USA, 16–19 June 2003; pp. 279–286.
13. Liu, J.; Liu, Y.-B.; He, X.; Liu, L. Study on TBCs insulation characteristics of a turbine blade under serving conditions. *Case Stud. Therm. Eng.* **2016**, *8*, 250–259. [CrossRef]
14. Prapamonthon, P.; Yooyen, S.; Sleesongsom, S.; DiPasquale, D.; Xu, H.; Wang, J.-H.; Ke, Z. Investigation of cooling performances of a non-film-cooled turbine vane coated with a thermal barrier coating using conjugate heat transfer. *Energies* **2018**, *11*, 1000. [CrossRef]
15. Prapamonthon, P.; Xu, H.; Yang, W.; Wang, J. Numerical study of the effects of thermal barrier coating and turbulence intensity on cooling performances of a nozzle guide vane. *Energies* **2017**, *10*, 362. [CrossRef]
16. Davidson, F.T.; Kistenmacher, D.A.; Bogard, D.G. Film cooling with a thermal barrier coating: Round holes, craters, and trenches. *J. Turbomach.* **2013**, *136*, 041007. [CrossRef]
17. Hylton, L.D.; Mihelc, M.S.; Turner, E.R.; Nealy, D.A.; York, R.E. *Analytical and Experimental Evaluation of the Heat Transfer Distribution Over the Surfaces of Turbine Vanes*; NASA Technical Report, NASA-CR-168015; NASA Lewis Research Center: Cleveland, OH, USA, 1982.

18. Hylton, L.D.; Nirmalan, V.; Sultanian, B.K.; Kauffman, R.M. *The Effects of Leading Edge and Downstream Film Cooling on Turbine Vane Heat Transfer*; NASA Technical Report, NASA-CR-182133; NASA: Washington, DC, USA, 1988.
19. Ke, Z.; Wang, J.-H. Conjugate heat transfer simulations of pulsed film cooling on an entire turbine vane. *Appl. Therm. Eng.* **2016**, *109*, 600–609. [CrossRef]
20. Jiang, Y.; Zheng, Q.; Dong, P.; Yao, J.; Zhang, H.; Gao, J. Conjugate heat transfer analysis of leading edge and downstream mist–air film cooling on turbine vane. *Int. J. Heat Mass Transf.* **2015**, *90*, 613–626. [CrossRef]



© 2020 by the authors. Licensee MDPI, Basel, Switzerland. This article is an open access article distributed under the terms and conditions of the Creative Commons Attribution (CC BY) license (http://creativecommons.org/licenses/by/4.0/).